On the net displacement of contact surface centroid in contractile bodies

José J. Muñoz^{1,2}, Lucie Condamin³, David Doste⁴

http://www.lacan.upc.edu/jose.munoz, j.munoz@upc.edu

Abstract

We investigate the motion of the contact surface centroid for contractile bodies on substrates with a viscous friction law and when inertial forces are negligible. We deduce a set of sufficient conditions that ensure that the surface centroid remains still. The conditions are automatically satisfied for linear analysis and homogeneous constant viscous friction parameters. In non-linear analysis additional requirements are necessary: i) the material is incompressible, ii) the material points in contact do not vary, and iii) the surface is flat. These results demonstrate the inability of slender organisms to move under homogeneous viscous contact condition if the contact surface remains constant, regardless of the contractility strategy employed. We numerically simulate some situations that do not comply to these conditions, such as the use of non-homogeneous or anisotropic friction, which illustrate possible strategies for net propulsion.

Keywords: centre of mass, locomotion, worm, friction, viscosity

1 Introduction

Mechanisms for locomotion of organisms have been well studied in fluids [8, 26] and granular media [5, 31]. However, only in the former case exist general principles for propulsion, which have been mainly derived for low Reynolds number [11, 23]. When bodies are submerged in a fluid, Purcell's scallop theorem furnishes sufficient conditions for the null net motion in fluids through the analysis of the parametric space of body configurations [22, 23]. In these results, Stokes equations are imposed, with a no-slip boundary condition.

Limbless self-propulsion of deformable solids on loose soil or granular matter has been analysed and modelled in detail [4, 12], and a theory that allows determining the propulsion from the interaction with the granular environment, so-called resistive force theory, has been derived and validated [13, 20, 12]. Moreover, optimal strategies for locomotion and cost reduction have been successfully deduced and simu-

lated [21, 17, 28]. However, partially due to the complex interaction at the boundary, no general equivalent theorem furnishing sufficient conditions for the no net motion of the body centroid (centre of mass when density is constant) on a frictional substrate has been established. This paper aims at furnishing some results along this direction.

In order to analyse the locomotion on a viscous frictional substrate, we assume a body Ω with the ability to self-contract and in contact with the substrate in a region $\partial\Omega_s$, as shown in Figure 1. Similar to the analysis in fluids, and due to the small size of Ω and the low accelerations, we neglect the contribution of inertial effects [16]. Eventually, we will consider thin or elongated organisms, such that in this case boundary forces can be approximated by body forces applied in the body domain Ω , which is initially occupying domain Ω_0 . We will also comment the situation when the whole limbless body is permanently in contact with the frictional substrate. The lifting or removal of friction will be discussed after deriving our main

¹Mathematics Department, Laboratori de Càlcul Numèric (LaCàN), Universitat Politècnica de Catalunya, Barcelona, Spain.

²Centre International de Mètodes Numèrics en Enginyeria (CIMNE), Barcelona, Spain.

³Institut National des Sciences Appliquées, Lyon, France.

⁴Facultat de Matemàtiques i Estadística, Universitat Politècnica de Catalunya, Barcelona, Spain.

results.

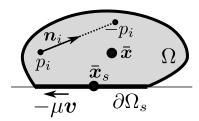


Figure 1: Schematic of a self contractile body Ω subjected to viscous friction at the bottom boundary and with contractile dipole $\pm p_i \mathbf{n}_i$. Large dots indicate body centroid $\bar{\mathbf{x}}$ and contact surface centroid \mathbf{x}_s .

2 Motion of contact surface centroid

We are interested in analysing the motion of the body centroid $\bar{x} = \int_{\Omega} x dV/V$, with volume $V = \int_{\Omega} dV$, and the motion of the contact surface centroid $\bar{x}_s = \int_{\Omega} x dS/S$, with $S = \int_{\partial \Omega_s} dS$. We will also denote by x and x_0 the position of a material point of body Ω in its current deformed position and in its reference configuration, respectively.

The ability to self-contract is represented by a field of N dipoles with opposing forces $\boldsymbol{f} = \sum_{i}^{N} \pm p_{i} \boldsymbol{n}_{i} \delta(\boldsymbol{x}_{i}^{\pm})$ and magnitude p_{i} , applied at points $\boldsymbol{x} = \boldsymbol{x}_{i}^{+}$ and $\boldsymbol{x} = \boldsymbol{x}_{i}^{-}$ along directions $\pm \boldsymbol{n}_{i} = \pm (\boldsymbol{x}_{i}^{+} - \boldsymbol{x}_{i}^{-})/||\boldsymbol{x}_{i}^{+} - \boldsymbol{x}_{i}^{-}||$, respectively. Note that the set of dipoles is indeed self-equilibrated, i.e.

$$\int_{\Omega} \boldsymbol{f} dV = \sum_{i}^{N} \pm p_{i} \boldsymbol{n}_{i} = \boldsymbol{0}.$$
 (1)

The static equilibrium of domain Ω is then given by Cauchy's equation, including the dipoles as a body force [6]:

$$\nabla \cdot \boldsymbol{\sigma} + \boldsymbol{f} = \boldsymbol{0}, \ \forall \boldsymbol{x} \in \Omega, \tag{2}$$

and with boundary conditions that we assume stemming from a viscous frictional condition

$$\sigma \boldsymbol{n} = -\mu \boldsymbol{v}, \quad \forall \boldsymbol{x} \in \partial \Omega_s, \sigma \boldsymbol{n} = \boldsymbol{0}, \qquad \forall \boldsymbol{x} \in \partial \Omega \backslash \partial \Omega_s.$$
 (3)

with $\mathbf{v} = \dot{\mathbf{x}}$ the material velocity. The associated weak form (or virtual principle) to problem (2)-(3) follows after pre-multiplying equation (2) by a set of compatible virtual displacements $\delta \mathbf{u}$, integrating by parts and considering the boundary condition in (3):

Find u such that, for all virtual admissible displacements δu ,

$$\int_{\Omega} \boldsymbol{\varepsilon}(\boldsymbol{\delta}\boldsymbol{u}) : \boldsymbol{\sigma}(\boldsymbol{u})dV = \pm \sum_{i} \boldsymbol{\delta}\boldsymbol{u} \cdot \boldsymbol{f}_{i}^{\pm}(\boldsymbol{x}_{i}^{\pm}) \\
- \int_{\partial\Omega_{\epsilon}} \mu \boldsymbol{\delta}\boldsymbol{u} \cdot \boldsymbol{v}dS, \quad (4)$$

with $\boldsymbol{\varepsilon}(\boldsymbol{\delta}\boldsymbol{u})$ the virtual strains. In linear analysis, $\boldsymbol{\varepsilon}(\boldsymbol{\delta}\boldsymbol{u}) = \frac{1}{2} \left(\nabla \boldsymbol{\delta}\boldsymbol{u} + (\nabla \boldsymbol{\delta}\boldsymbol{u})^T \right)$, while in finite strains and large displacements, $\boldsymbol{\varepsilon}(\boldsymbol{\delta}\boldsymbol{u}) = \mathbf{F}^{-T}\boldsymbol{\delta}\mathbf{E}\mathbf{F}^T$, with $\mathbf{E} = \frac{1}{2} \left(\mathbf{F}^T\mathbf{F} - \mathbf{I} \right)$) the Lagrangian or Green strain tensor, and the deformation gradient \mathbf{F} defined by $\mathbf{F} = \frac{\partial \boldsymbol{x}}{\partial \boldsymbol{x}_0}$ [6].

The equality in (4) must hold for all compatible virtual displacements δu , which in our case includes a constant displacement $\delta \hat{u}$. Therefore, since $\varepsilon(\delta \hat{u}) = 0$ and the dipoles are self-equilibrated (see equation (1)), equation (4) implies the following relation,

$$\int_{\partial\Omega_s} \mu \mathbf{v} dS = \mathbf{0}. \tag{5}$$

In linear analysis, where $dS \approx dS_0$, and with constant homogeneous viscosity, this equation implies that the position of the contact surface centroid \bar{x}_s is constant. In order to show that in general non-linear analysis this is not so, we recall Nanson's formula [15], $dS\mathbf{n} = J dS_0\mathbf{F}^{-T}\mathbf{N}$, with (dS, \mathbf{n}) and (dS_0, \mathbf{N}) the surface differential and normal vectors in the deformed and reference configuration, respectively, and $J = det(\mathbf{F})$. By using also the relations $J = (\nabla \cdot \mathbf{v})J$ and $\dot{\mathbf{F}}^{-1} = -\mathbf{F}^{-1}\nabla\mathbf{v}$, it then follows that the time variation of the surface differential can be expressed as,

$$\dot{dS} = (\nabla \cdot \boldsymbol{v})dS + JdS_0 \left(\dot{\boldsymbol{n}} - \nabla \boldsymbol{v} \boldsymbol{n}\right) \cdot \mathbf{F}^{-T} \boldsymbol{N}
= (\nabla \cdot \boldsymbol{v})dS + dS \left(\dot{\boldsymbol{n}} - \nabla \boldsymbol{v} \boldsymbol{n}\right) \cdot \boldsymbol{n}.$$
(6)

As a consequence,

$$\dot{\bar{x}}_s = \int_{\partial\Omega_s} \boldsymbol{v} dS + \int_{\partial\Omega_s} \boldsymbol{x} (\nabla \cdot \boldsymbol{v}) dS
+ \int_{\partial\Omega_s} \boldsymbol{x} (\dot{\boldsymbol{n}} - \nabla \boldsymbol{v} \boldsymbol{n}) \cdot \boldsymbol{n} dS.$$
(7)

From this expression, we can deduce a set of conditions that together, ensure the motion of the contact surface centroid vanishes:

- i) The friction coefficient μ is constant and homogeneous.
- ii) The material is incompressible.
- iii) The material points that are in contact with the substrate remain in contact.
- iv) The substrate is flat.

Conditions i) and ii) are very common in many $in\ vitro$ situations in biomechanics. These, together with the result in (5), imply that the first two terms in the rhs of (7) vanish. As a consequence of condition iii), $\mathbf{n} \cdot \partial_n \mathbf{v} = \mathbf{n} \cdot \nabla \mathbf{v} \mathbf{n} = \mathbf{0}$, that is, the material region $\partial \Omega_s$ is constant, while condition iv) yields $\dot{\mathbf{n}} = \mathbf{0}$. Summarising, when conditions i)-iv) are satisfied, we have that,

$$\dot{\bar{x}}_s = \mathbf{0}.\tag{8}$$

3 Discussion

In deriving the result in (8) we have determined sufficient kinematic and frictional conditions for the null motion of the contact surface centroid. We recognise that some of them were expected, such as the requirement of homogeneous and constant friction on flat surfaces, or having no variations of the normal velocity across the contact surface, so that the contact surface is maintained. However, other particular conditions that may give rise to contact surface net motion, such as compressibility or using a non-flat surface, even when viscosity is constant and homogeneous, are less evident.

Considerable work has been devoted to the analysis of sufficient conditions for locomotion of immersed

bodies, where organisms are subjected to friction or no-slip conditions on the whole surface [11, 22]. However, a similar analysis of the sufficient conditions for no net motion when the body is partially in contact with a viscous substrates has not been analysed, to the authors' knowledge, although some of the sufficient conditions for locomotion have been well studied [4, 8].

For instance, for flat or elongated shapes, and when nearly the whole body is in contact with the substrate, body and contact surface centroids are approximately equivalent, i.e. $\bar{x}_s \approx \bar{x}$. Net motion of \bar{x} may be then achieved by varying the contact surface in different regions of the boundary, like in sidewinding [4]. Our first example in the next section simulates such situation.

We emphasise that relation (5) shows that the surface centroid does not move in linear analysis and when $\mu = const > 0$. For more general contact friction laws with the form $\sigma n = -\mu(v)$, the result in equation (5) must be replaced by,

$$\int_{\partial\Omega} \boldsymbol{\mu}(\boldsymbol{v}) dS = \mathbf{0}. \tag{9}$$

This relation does not imply the immobility of \bar{x}_s , and in consequence, diversions from the homogeneous constant frictional condition may give rise to changes in \bar{x}_s . Some examples are the use of different parallel and normal frictional coefficients, as employed in the resistive force theory [24, 13, 20], or resorting to different coefficients in different tangential directions, as it is the case of euglenoids in fluids [1].

We point out that relation (8) is valid for any contractile strategy and material constitutive law. For the particular case of elastic bodies, the result in (8) can be interpreted as the solution of minimising a total energy functional. For showing this, we first discretise the weak form in (4) with a time-stepping $\mathbf{v}_{n+1} \approx (\mathbf{u}_{n+1} - \mathbf{u}_n)/(t_{n+1} - t_n)$. The displacement at time t_{n+1} , denoted by \mathbf{u}_{n+1} is then equivalent to finding the minimiser of a functional $W(\mathbf{u}_{n+1})$ given

by

$$W(\boldsymbol{u}_{n+1}) = \int_{\Omega} \phi(\boldsymbol{u}_{n+1}) dV + \sum_{i} p_{i} l_{i}(\boldsymbol{u}_{n+1})$$
$$+ \frac{1}{2(t_{n+1} - t_{n})} \int_{\partial \Omega} \mu ||\boldsymbol{u}_{n+1} - \boldsymbol{u}_{n}||^{2} dS,$$

with $l_i(\boldsymbol{u}) = ||\boldsymbol{x}_i^+ - \boldsymbol{x}_i^-||$ the length of the dipole, and $\phi(\boldsymbol{u})$ an elastic energy density function. By noting that both $l_i(\boldsymbol{u})$ and $\phi(\boldsymbol{u})$ are invariant with respect to rigid body motions, and splitting the displacement \boldsymbol{u}_{n+1} into the surface mean value $\bar{\boldsymbol{u}}_s$ and the deviation $\Delta \boldsymbol{u}_s$, that is, by writing $\boldsymbol{u}_{n+1} = \bar{\boldsymbol{u}}_s + \Delta \boldsymbol{u}_s$, with $\bar{\boldsymbol{u}}_s = \int_{\partial\Omega} \boldsymbol{u}_{n+1} dS/S$, it can be shown that with the same conditions i)-iv), we have that

$$W(\boldsymbol{u}_{n+1}) = W(\Delta \boldsymbol{u}_s) + \mu ||\bar{\boldsymbol{u}}_s||^2 S.$$
 (10)

Since the solution u_{n+1} minimises $W(u_{n+1})$, the surface mean value must vanish, i.e. $\bar{u}_s = 0$.

4 Numerical Examples

We illustrate our results with a couple of examples that will be solved numerically. The first one consists on a flat square domain $[0,L]^2$ in contact with a substrate, and contracting according to the following two strategies: a) constant friction everywhere with an applied local contractility along a thin vertical domain (see Figure 2a), and b) a contraction on the whole domain with a null friction along a thin vertical line (see Figure 2b). We test different horizontal positions c of the contracting band in case a) and different positions of the frictionless band in case b). The problem is solved resorting to a finite element discretisation and the contraction is implemented by superimposing to the elastic deformation an isotropic contractile strain $\varepsilon^c \mathbf{I}$.

The numerical results confirm that in both cases the displacement of the centroid of the surface that has non-zero friction vanishes, i.e. $\bar{u}_s = 0$, for any contractile strategy in case a), and for each one of the friction distributions in case b). We show in Figure 3 the plot of \bar{u} for different locations of the contractile band in case a) and for each location of the frictionless band in case b). In case a), since the frictional

surface also coincides with the whole body surface, we have that $\bar{u}=\mathbf{0}$ for all values of c. Instead, in case b), since the centre of the frictional surface is moving backwards as c increases, the centre of the whole body \bar{x} moves forwards for c < L/2, while \bar{x} moves backwards for c > L/2. When c = L/2, the two centres coincide, $\bar{x}_s = \bar{x}$, and in this case no net displacement of the body centre is obtained, i.e. $\bar{u} = \bar{u}_s = \mathbf{0}$.

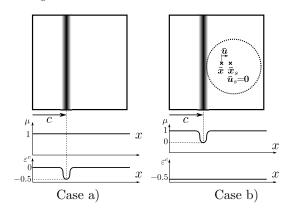


Figure 2: Example 1: Contractile square domain. a) Homogeneous friction with a localised contractility on a vertical band. b) Homogeneous contractility with a localised reduction of friction on a vertical band.

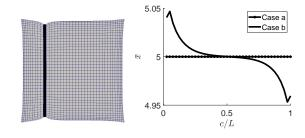


Figure 3: Example 1: Left: deformation for case b. Right: resulting displacement of motion of horizontal coordinate of the body (surface) centre.

In a second example, we analyse a worm-like unidimensional domain that has the ability to bend and produce a wave-like undulation, similarly to the analysis presented for hydrodynamics in [29]. The worm is modelled here as a set of n planar line segments joining n+1 nodes x_0, \ldots, x_n . Stretching and bending elasticity is furnishing by using the following total elastic potential

$$\Phi(\boldsymbol{x}) = \sum_{i=0}^{n} k(||\boldsymbol{x}_{i+1} - \boldsymbol{x}_{i}|| - l_{i0})^{2} + \sum_{i=1}^{n} k_{\theta} \sin^{2} \theta_{i},$$

with l_{i0} the initial length of segment $\boldsymbol{x}_{i+1} - \boldsymbol{x}_i$ and θ_i the angle between $\boldsymbol{x}_{i+1} - \boldsymbol{x}_i$ and $\boldsymbol{x}_i - \boldsymbol{x}_{i-1}$ (see Figure 4). In addition to the elastic forces, the model is subjected to nodal frictional components $\boldsymbol{f}_i^\mu = -\mu \boldsymbol{v}_i$ and a set of bending moments M_i applied at the interior nodes $i=1,\ldots,n-1$. Each bending moment M_i is in fact decomposed into three self-equilibrated forces $\boldsymbol{f}_i^-, \boldsymbol{f}_i^o, \boldsymbol{f}_i^+$, respectively applied at nodes $\boldsymbol{x}_{i-1}, \boldsymbol{x}_i$ and \boldsymbol{x}_{i+1} . These forces are normal to direction $\boldsymbol{x}_{i+1} - \boldsymbol{x}_{i-1}$, and such that $\boldsymbol{f}_i^- + \boldsymbol{f}_i^o + \boldsymbol{f}_i^+ = \boldsymbol{0}$, with a resulting bending moment equal to M_i , as also illustrated in Figure 4(left). More specifically, the relation between M_i and the three nodal forces is given by:

$$0 = f_i^- + f_i^o + f_i^+$$

$$0 = \mathbf{e}_z \cdot (f_i^- (\mathbf{x}_{i-1} - \mathbf{x}_i) + f_i^- (\mathbf{x}_{i+1} - \mathbf{x}_i)) \times \mathbf{n}_i$$

$$M_i = \mathbf{e}_z \cdot (f_i^- (\mathbf{x}_{i-1} - \mathbf{x}_i) - f_i^- (\mathbf{x}_{i+1} - \mathbf{x}_i) \times \mathbf{n}_i) \times \mathbf{n}_i$$
(11)

with $\mathbf{e}_z = \{0, 0, 1\}^T$ and $\mathbf{n}_i = \mathbf{e}_z \times (\mathbf{x}_{i+1} - \mathbf{x}_{i-1})/||\mathbf{x}_{i+1} - \mathbf{x}_{i-1}||$ the approximated normal vector at node i. These conditions define uniquely the direction and magnitude of the forces for a given value of M_i . The equilibrium equations for each node i read then,

$$\frac{\partial \Phi(\boldsymbol{x})}{\partial \boldsymbol{x}_i} + \boldsymbol{f}_i^M = \boldsymbol{f}_i^\mu, \tag{12}$$

where vector $\boldsymbol{f}_i^M = \boldsymbol{f}_{i-1}^+ + \boldsymbol{f}_i^o + \boldsymbol{f}_{i+1}^-$ includes all the force contributions at node i due to the contractile bending moments. We have applied a distribution of time varying moments equal to

$$M_i = \sin(\omega t - ks_i),$$

except at the end points, where $M_0 = M_n = 0$. Here, ω is the frequency, k the wave number, and s_i the initial position of point x_i . The discretised weak form

of the balance equations in (12) reads,

Find u_i such that for all virtual displacements δu_i

$$oldsymbol{\delta u}_i \cdot rac{\partial \Phi(oldsymbol{x})}{\partial oldsymbol{x}_i} + oldsymbol{\delta u}_i \cdot oldsymbol{f}_i^M = oldsymbol{\delta u}_i \cdot oldsymbol{f}_i^\mu.$$

Since this relation must be also satisfied for arbitrary rigid body displacements, and we also have that $\sum_{i} \boldsymbol{f}_{i}^{M} = \mathbf{0}$ (forces due to applied moments are self-equilibrated by construction, according to (11)) and $\sum_{i} \frac{\partial \Phi}{\partial x_{i}} = \mathbf{0}$, we have an equivalent result to the one in (5):

$$\sum_{i} \mu \boldsymbol{v}_{i} = \boldsymbol{0}.$$

For a constant viscous coefficient, this result implies that the mean velocity also vanishes. We have numerically solved the set of n non-linear equations in (12), and verified that when isotropic friction is used, the resulting motion of the worm centre $\dot{\bar{x}} = \sum_i v_i/n$ is exactly zero, up to machine tolerance. When the same oscillatory set of moments is used, but in conjunction with anisotropic friction $f^{\mu} = -\mu_t v_t - \mu_n v_n$, with v_t and v_n the tangential and normal components of the displacements, and μ_t and μ_n two different friction coefficients, the worm is propelled, as shown in Figure 4 (right). In this case, the worm centre moves in the opposing direction of the wave of bending moments, as also pointed out for locomotion in fluids [8, 11] and solids [12].

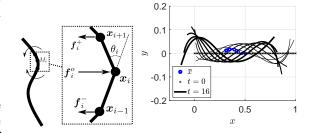


Figure 4: Example 2: Left: Worm-like domain with self-contractile moments. Right: Snapshots of deformed shape for anisotropic friction ($\mu_n = 10\mu_t = 1$).

We have tested different frequencies ω and wave numbers k. The sequence of horizontal displacements shown in Figure 5 indicates that although final displacement increases for increasing values of ω and k, there is for both parameters a limit value beyond which no substantial improvement is observed. This fact is also confirmed by the low wave numbers and limited frequencies that organisms generally exhibit [12]. We have not focused this study on the search of optimal modes or strategies, also with respect to other motion parameters such as amplitude or friction, which have been analysed elsewhere [5, 18, 32, 14], or simulated with the discrete element method [10]. We intend to analyse in future works more realistic resistive forces such as frictional plasticity models [2], or more complex waves such as those in sidewinding [3] or helical motion [31], and interpret them as a drift from the homogeneous frictional conditions where no motion is achieved.

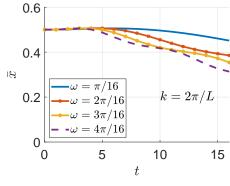
5 Conclusions

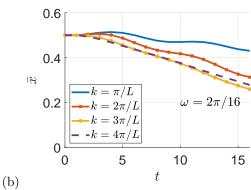
We have derived a set of sufficient conditions for maintaining the contact surface centroid at rest. The two examples presented above exploit the violations of some of these conditions, giving rise to net propulsion. The first example uses a reduction of friction in some regions of the contact surface, while the second example resorts to anisotropic friction. These are in contrast with some well-known conditions required for achieving locomotion in fluids, such as the non-time reversibility of the body deformations [8, 22, 11].

In one of our numerical examples we obtain propulsion by reducing friction on a subdomain of the body surface. The resulting centroid displacement is similar to the one studied in fluids when a contractile wave. In our case though, the net movement is not the result of alternating vortices [11], but rather a difference between the positions of the body centroid \bar{x} , and the contact surface centroid \bar{x}_s .

We remark that our theoretical results are applicable to solids with arbitrary constitutive laws and contractile strategies, and applicable to large displacements and deformations. However, our conclusions cannot be generalised to bodies immersed in a fluid, where a no-slip condition is assumed in this case.

We also mention that our analysis is pertinent to





(a)

Figure 5: Example 2. (a) Horizontal displacement of the worm centroid for increasing values of frequency. (b) Horizontal displacement of the worm centroid for increasing values and wave number .

crawling microorganisms on frictional substrates such as *C. elegans* on agar [25, 8]. In many instances, net locomotion is achieved through the activation of contractile waves, as it is the case in lateral undulation and sidewinding, with some lifting/lowering, which results in a variation of the frictional conditions. While the measurement of the centre of mass in swimming organisms [33] and human gait dynamics [30] is common, its analysis and correlation with substrate friction at cell mechanics is usually not investigated.

Indeed, understanding sufficient conditions for the null net movement may help to elucidate the conditions for migration in cells or monolayers on substrates, where planar motion is dominant *in vitro*.

For instance, substantial computational and experimental efforts have been devoted to traction force microscopy (retrieval of traction field exerted by cells or tissues) [7, 9, 19, 27]. In those cases, the motion of the tissue centre should be interpreted as a set of unequal adhesions, and not solely to differential tissue contractility. Accordingly, the configurational parametric space should be analysed jointly with modes of the contact conditions.

References

- M. Arroyo, L. Heltai, D. Millan, and A. Desimone. Reverse engineering the euglenoid movement. *Proc. Natl. Acad. Sci. USA*, 109(44):17874–17879, 2012.
- [2] H. Askari and K. Kamrin. Intrusion rheology in grains and other flowable materials. *Num. Math.*, 15:1274–1270, 2016.
- [3] H. C. Astley, C. Gong, J. Dai, M. Travers, M. M. Serrano, P. A. Vela, H. Choset, J. R. Jr. Mendelson, D. L. Hu, and D. I. Goldman. Modulation of orthogonal body waves enables high maneuverability in sidewinding locomotion. *Proc. Natl. Acad. Sci. USA*, 112:6200–6205, 2015.
- [4] H.C. Astley, J.R. Mendelson, J. Dai, C. Gong, B. Chong, J.M. Rieser, P.E. Schiebel, S.S. Sharpe, R.L. Hatton, H. Choset, and D.I. Goldman. Surprising simplicities and syntheses in limbless self-propulsion in sand. *J. Exp. Biol.*, 223:103564, 2020.
- [5] J.E. Avron, O. Gat, and O.Kenneth. Optimal swimming at low reynolds numbers. *Phys. Rev.* E, 93:186001, 2004.
- [6] J. Bonet and R.D. Wood. Non-linear continuum mechanics for finite element analysis. Cambridge University Press, 1997.
- [7] J.P. Butler, I.M. Tolić-Nørrelykke, B. Fabry, and J.J. Fredberg. Traction field, moments, and strain energy that cells exert on their surroundings. Amer. J. Physiol. Cell Physiol., 282:C595— C605, 2002.

- [8] N. Cohen and J.H. Boyle. Swimming at low reynolds number: a beginners guide to undulatory locomotion. *Cont. Phys.*, 29:103–123, 2010.
- [9] JC del Álamo, R Meili, B Álvarez-González, B Alonso-Latorre, E Bastounis, R Firtel, and JC Lasheras. Three-dimensional quantification of cellular traction forces and mechanosensing of thin substrata by Fourier traction force microscopy. PLoS ONE, 8(9):e69850, 2013.
- [10] Y. Ding, S. S. Sharpe, A. Masse, and D. I. Gold-man. Mechanics of undulatory swimming in a frictional fluid. *PLOS Comp. Biol.*, 8:e1002810, 2012.
- [11] E.Lauga and T.R. Powers. The hydrodynamics of swimming microorganisms. *Rep. Prog. Phys.*, 72:096601, 2009.
- [12] D. I. Goldman. Colloquium: biophysical principles of undulatory selfpropulsion in granular media. Rev. Modern Phys., 86:943–958, 2014.
- [13] J. Gray and G. J. Hancock. The propulsion of sea-urchin spermatozoa. J. Exp. Biol., 32:802, 1955.
- [14] R. L. Hatton, Y. Ding, H. Choset, and D. I. Goldman. Geometric visualization of selfpropulsion in a complex medium. *Phys. Rev.* Letters, 110(7):078101, 2013.
- [15] G.A. Holzapfel. Nonlinear solid mechanics. A continuum approach for engineers. J Wiley & Sons Ltd, Chichester., 2000.
- [16] D.L. Hu, J. Nirody, T. Scott, and M.J. Shelley. The mechanics of slithering locomotion. *Proc. Natl. Acad. Sci. USA*, 106:10081–10085, 2009.
- [17] Z. Jiang and J. Xu. Analysis of worm-like locomotion driven by the sine-squared strain wave in a linear viscous medium. *Mech. Res. Comm.*, 85:33–44, 2017.
- [18] T. Kano, R. Kobayashib, and A. Ishiguro. Decentralized control scheme for adaptive earthworm locomotion using continuum-model-based analysis. Adv. Robotics, 28(3):197–202, 2014.

- [19] WR Legant, CK Choi, JS Miller, L Shao, L Gao, E Betzig, and CS Chen. Multidimensional traction force microscopy reveals out-of-plane rotational moments about focal adhesions. *Proc.* Natl. Acad. Sci. USA, 110(3):881–886, 2013.
- [20] R. D. Maladen, Y. Ding, C. Li, and D. I. Gold-man. Undulatory swimming in sand: Subsurface locomotion of the sandfish lizard. *Science*, 325:314–318, 2009.
- [21] G. Noselli, A. Tatone, and A. DeSimone. Discrete one-dimensional crawlers on viscous substrates: Achievable net displacements and their energy cost. *Mech. Res. Comm.*, 58:73–81, 2014.
- [22] E.M. Purcell. Live at low Reynolds number. *Amer. J. Phys.*, 45(1):3–11, 1977.
- [23] A. Shapere and F. Wilczek. Geometry of selfpropulsion at low reynolds number. *J. Fluids Mech.*, 198:557–685, 1989.
- [24] S. S. Sharpe, S. A. Koehler, R. M. Kuckuk, M. Serrano, P. A. Vela, J. Mendelson, and D. I. Goldman. Locomotor benefits of being a slender and slick sand swimmer. J. Exp. Biol., 218:440– 450, 2015.
- [25] G.J. Stephens, B. Johnson-Kerner, W. Bialek, and W.S. Ryu. Dimensionality and dynamics in the behavior of c. elegans. PLOS Comp. Biol., 4:e1000028, 2008.
- [26] H.A. Stone and A.D.T. Samuel. Propulsion of microorganisms by surface distortions. *Phys. Rev. Letters*, 77(19):4102–4104, 1996.
- [27] R. Sunyer, V. Conte, J. Escribano, A. Elosegui-Artola, A. Labernadie, L. Valon, D. Nava-jas, J.M. García-Aznar, J.J. Muñoz, P. Roca-Cusachs, and X. Trepat. Collective cell durotaxis emerges from long-range intercellular force transmission. *Science*, 353(6304):1157–1161, 2016.
- [28] Y. Tanaka1, K. Ito, T. Nakagaki, and R. Kobayashi. Mechanics of peristaltic locomotion and role of anchoring. J. R. Soc. Interface, 9:222–233, 2012.

- [29] G.I. Taylor. Analysis of the swimming of microscopic organisms. *Proc. Royal Soc. A*, 209:447—611, 1951.
- [30] L. Tesio, V. Rota, C. Chessa, and L. Perucca. The 3d path of body centre of mass during adult human walking on force treadmill. *J. Biome*chanics, 43:938–944, 2010.
- [31] B. D. Texier, A. Ibarra, and F. Melo. Helical locomotion in a granular medium. *Phys. Rev.* Letters, 119(6):068003, 2017.
- [32] J.L. van Leeuwen, C.J. Voesenek, and U.K. Muller. How body torque and Strouhal number change with swimming speed and developmental stage in larval zebrafish. *J. R. Soc. Interface*, 12(110):20150479, 2015.
- [33] G. Xiong and G.V. Lauder. Center of mass motion in swimming fish: effects of speed andlocomotor mode during undulatory propulsion. *Zool.*, 117:269–281, 2014.